

Supplementary Information

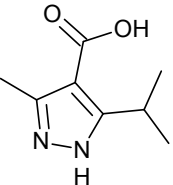
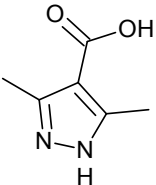
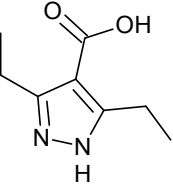
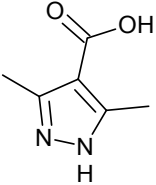
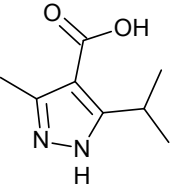
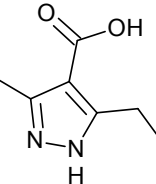
Hierarchical structuring of metal-organic framework thin-films on quartz crystal microbalance (QCM) substrates for selective adsorption and sensing applications

Suttipong Wannapaiboon,^a Min Tu,^a Kenji Sumida,^b Kira Khaletskaya,^a Shuhei Furukawa,^b Susumu Kitagawa,^b and Roland A. Fischer*^a

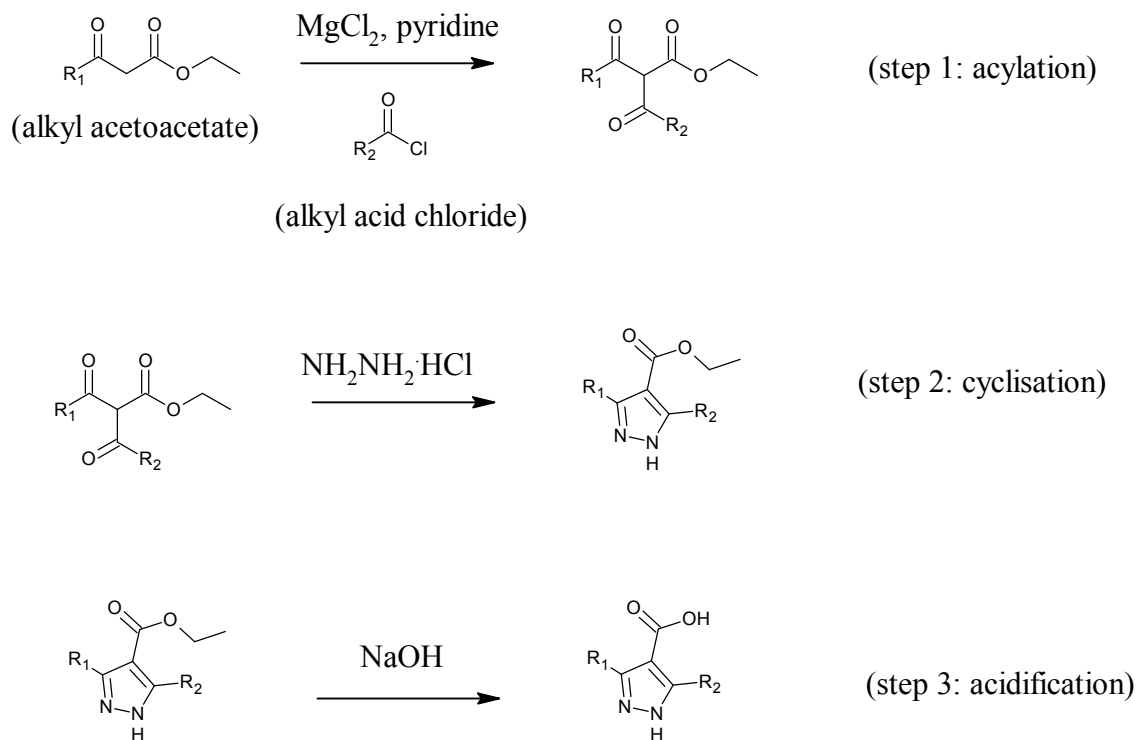
^a Chair of Inorganic Chemistry II - Organometallics and Materials Chemistry, Ruhr-University Bochum, D-44780 Bochum, Germany. Fax: +49(0) 234-32-14174; Tel: +49(0) 234-32-23629; E-mail: roland.fischer@rub.de

^b Institute for Integrated Cell-Material Sciences (WPI-iCeMS), Kyoto University, Yoshida, Sakyo-ku, Kyoto 606-8501, Japan. Fax: +81(0) 75-753-9820; Tel: +81(0) 75-753-9868

Table S1 Heterostructured shell-on-core [Zn₄O(3,5-dialkylcarboxypyrazolate)₃]_n MOF thin films reported in this study

Heterostructured shell-on-core MOF films	Organic linkers used for the thin film fabrication at	
	Shell (outer layer)	Core (inner layer)
1. Zn-MI-on-Zn-DM		
<ul style="list-style-type: none">• Zn-MI(10)-on-Zn-DM(20)• Zn-MI(15)-on-Zn-DM(20)• Zn-MI(20)-on-Zn-DM(20)• Zn-MI(10)-on-Zn-DM(30)• Zn-MI(15)-on-Zn-DM(30)• Zn-MI(20)-on-Zn-DM(30)		
2. Zn-DE-on-Zn-DM		
<ul style="list-style-type: none">• Zn-DE(10)-on-Zn-DM(20)• Zn-DE(20)-on-Zn-DM(20)• Zn-DE(10)-on-Zn-DM(30)• Zn-DE(20)-on-Zn-DM(30)		
3. Zn-MI-on-Zn-ME		
<ul style="list-style-type: none">• Zn-MI(20)-on-Zn-ME(20)• Zn-MI(20)-on-Zn-ME(30)		

Note: the number in the blanket is the number of deposition cycles



Scheme S1 Schematic reactions for syntheses of 3-alkyl-5-alkyl-4-carboxypyrazole functionalised linker: 3,5-dimethyl-4-carboxypyrazole (H₂DM, R₁ = R₂ = methyl), 3-methyl-5-ethyl-4-carboxypyrazole (H₂ME, R₁ = methyl, R₂ = ethyl), 3-methyl-5-isopropyl-4-carboxypyrazole (H₂MI, R₁ = methyl, R₂ = isopropyl) and 3,5-diethyl-4-carboxypyrazole (H₂DE, R₁ = R₂ = ethyl)

Note:

- 3,5-dimethyl-4-carboxypyrazole (H₂DM): ¹H NMR (250 MHz, CD₃OD) δ 2.41 (6H, s)
- 5-methyl-3-ethyl-4-carboxypyrazole (H₂ME): ¹H NMR (200 MHz, CD₃OD) δ 2.78 (2H, q), 2.32 (3H, s), 1.12 (3H, t)
- 5-methyl-3-isopropyl-4-carboxypyrazole (H₂MI): ¹H NMR (200 MHz, CD₃OD) δ 3.64 (1H, sep), 2.41 (3H, s), 1.26 (6H, d).
- 3,5-diethyl-4-carboxypyrazole (H₂DE): ¹H NMR (200 MHz, CD₃OD) δ 2.89 (4H, q), 1.23 (6H, t)

Calculation of specific adsorption amount by quartz crystal microbalance (QCM)

The mass of the deposited MOF thin film was calculated by the difference in the fundamental QCM oscillation frequency (F_0) and the frequency after final activation of the MOF film sample according to the Sauerbrey equation^[1](equation 1).

$$\Delta F = -\frac{2F_0^2}{A\sqrt{\mu \cdot \rho}} \cdot \Delta M \quad (1)$$

F_0 : fundamental frequency, A : surface area of electrode, μ : shear stress of quartz (2.947×10^{10} kg·m⁻¹·s⁻²) and ρ : density of quartz (2648 kg·m⁻³).

The mass uptake on the QCM substrate owing to the adsorption or desorption of the probe organic vapor on the surface-mounted MOF films (ΔM) could be also achieved from the change of resonance frequency according to the Sauerbrey equation. Consequently, the adsorption amount at each relative vapour pressure can be derived as shown in equation 2.

$$\text{Adsorption amount (g/g):} \quad \frac{\Delta M}{M_0} = \frac{F - F_s}{F_s - F_0} \quad (2)$$

M_0 : initial weight of the MOF film sample, F : measuring frequency at each relative vapour pressure and F_s : frequency after final activation of the MOF film sample.

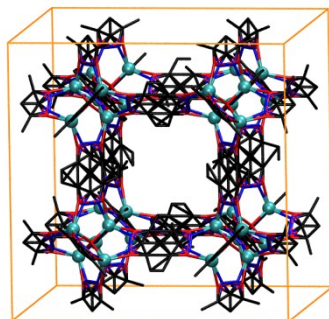


Figure S1 Schematic crystal structure of $[\text{Zn}_4\text{O}(\text{3,5-dimethyl-4-carboxypyrazolate})_3]_n$ MOF (**Zn-DM**) in the cubic $Fm-3m$ space group^[2]

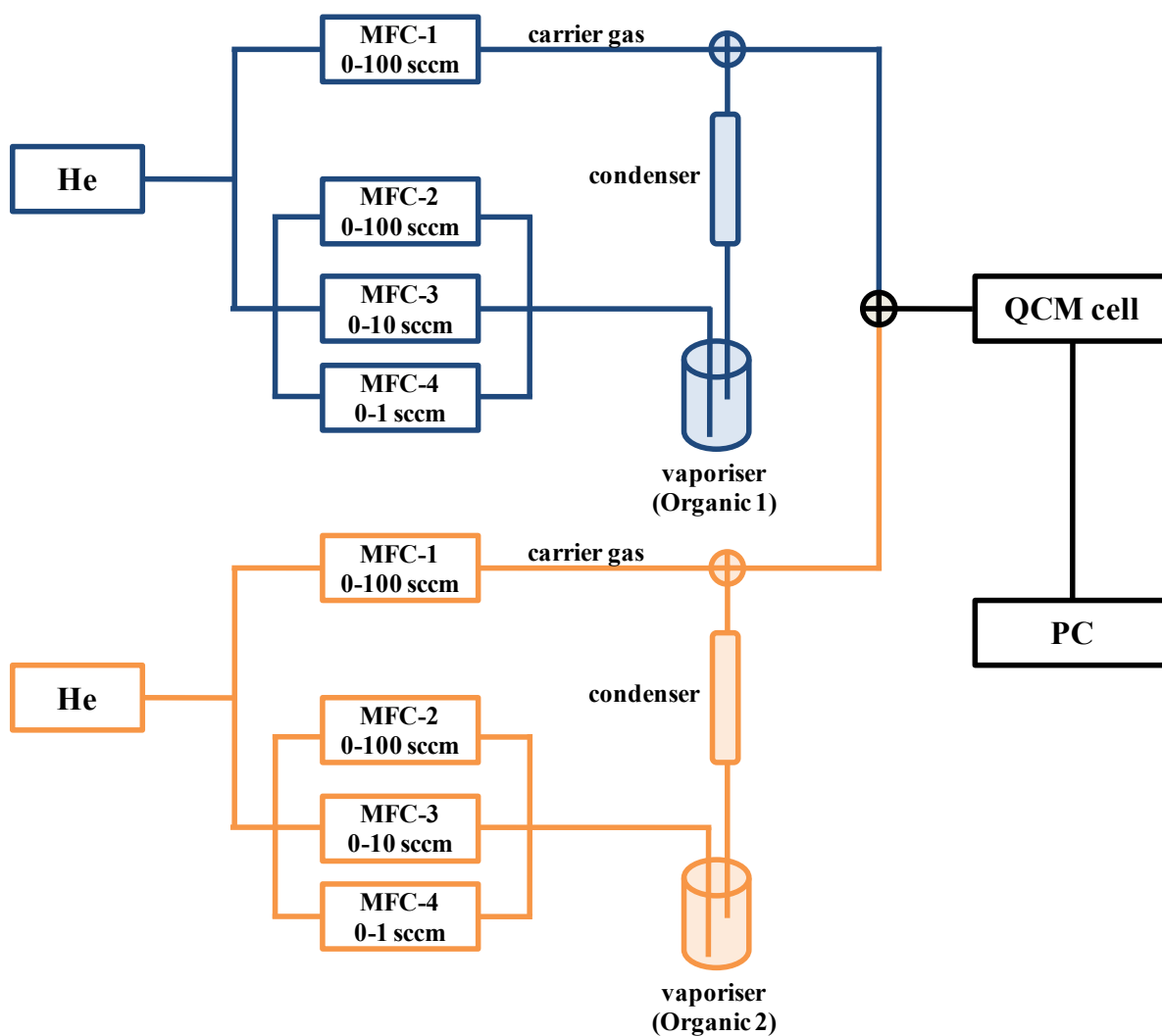


Figure S2 Schematic representation of experimental setup for multiple vapour sorption experiments using an environmental controlled quartz crystal microbalance (BEL-QCM). For the single vapour sorption experiments, only one set of mass flow controllers, vaporiser and condenser is used. The total gas flow to the QCM cell is 100 sccm.

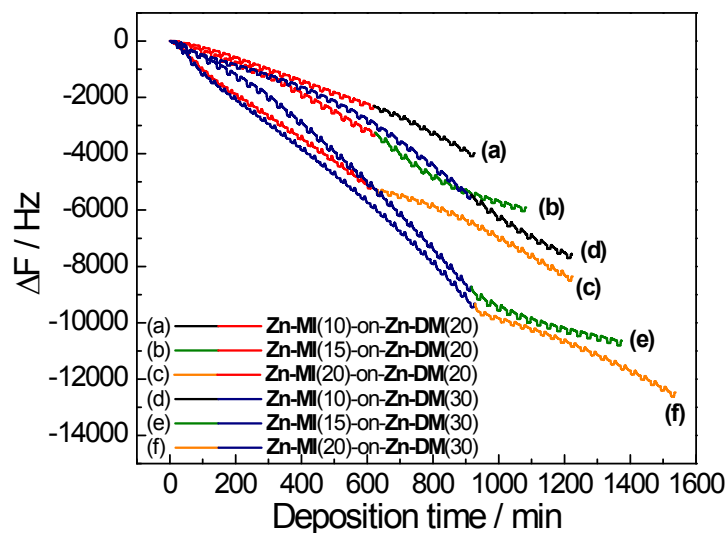


Figure S3 In-situ monitoring of the changing of QCM frequency as a function of deposition time during the continuous liquid phase epitaxial (LPE) growths of the **Zn-MI-on-Zn-DM** heterostructured films with various number of deposition cycles in each MOF component.

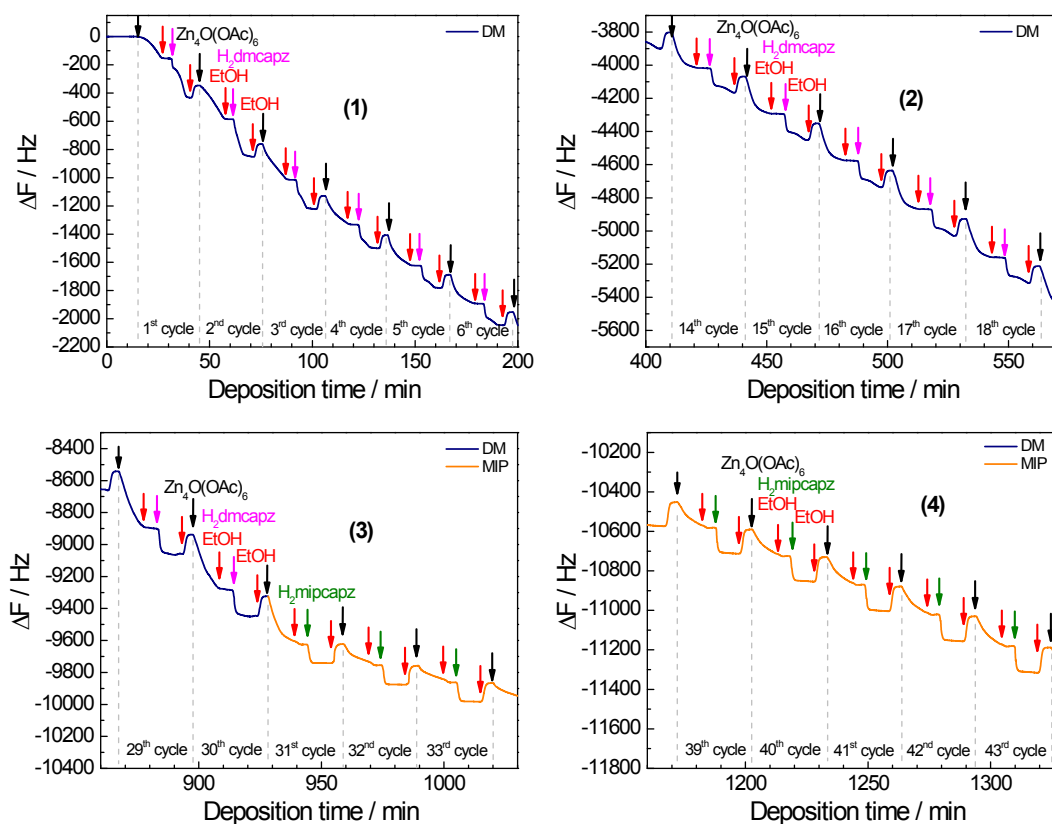


Figure S4 In-situ monitoring of the changing of QCM frequency as a function of deposition time during the continuous LPE growth of the **Zn-MI(20)-on-Zn-DM(30)** heterostructured film at different sections corresponding to the growth curve in Figure S3 (f).

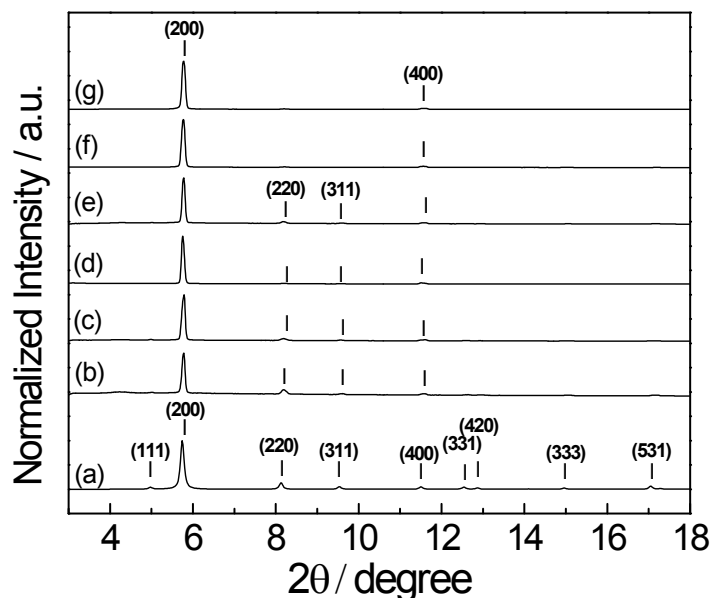


Figure S5 (a) Simulated powder X-ray diffraction pattern for bulk **Zn-DM** ($\lambda = 1.00130 \text{ \AA}$); and out-of-plane cuts from 2D-grazing incidence X-ray diffraction (GIXRD) patterns using a synchrotron source ($\lambda = 1.00130 \text{ \AA}$) for (b) **Zn-MI(20)-on-Zn-ME(20)**, (c) **Zn-MI(20)-on-Zn-ME(30)**, (d) **Zn-DE(10)-on-Zn-DM(20)**, (e) **Zn-DE(20)-on-Zn-DM(20)**, (f) **Zn-DE(10)-on-Zn-DM(30)**, and (g) **Zn-DE(20)-on-Zn-DM(30)**. The numbers within the parentheses in the figure indicate the Miller indices of the crystal planes.

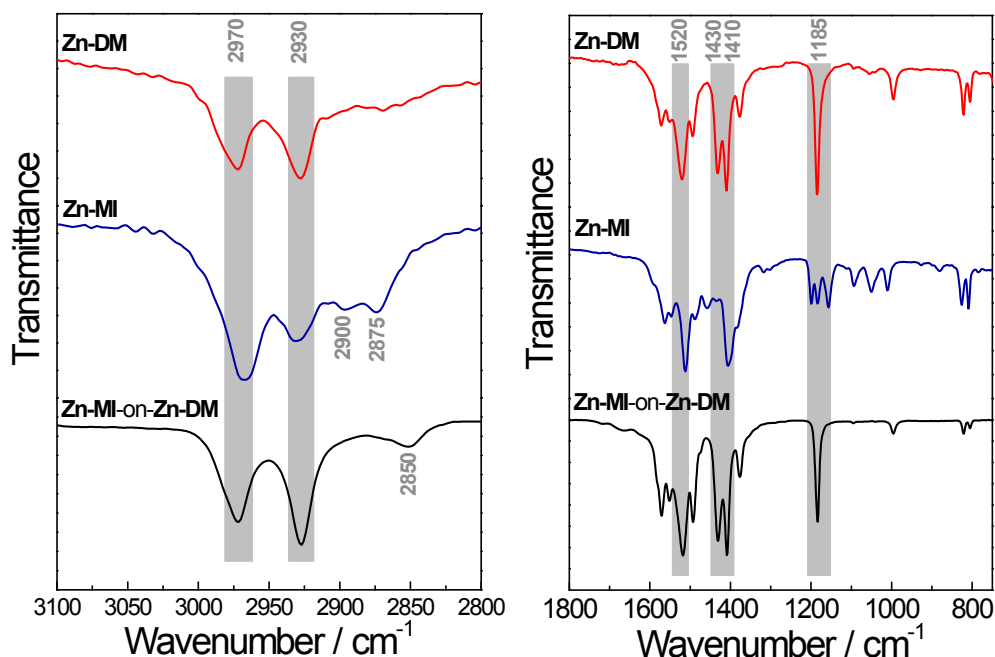


Figure S6 Example of IRRAS spectra of **Zn-MI-on-Zn-DM** heterostructured films indicates the position of the IR vibrational signals and the variation of relative transmittance at some wave numbers as a combination between the IRRAS spectra of the corresponding **Zn-DM** and **Zn-MI** MOF films.

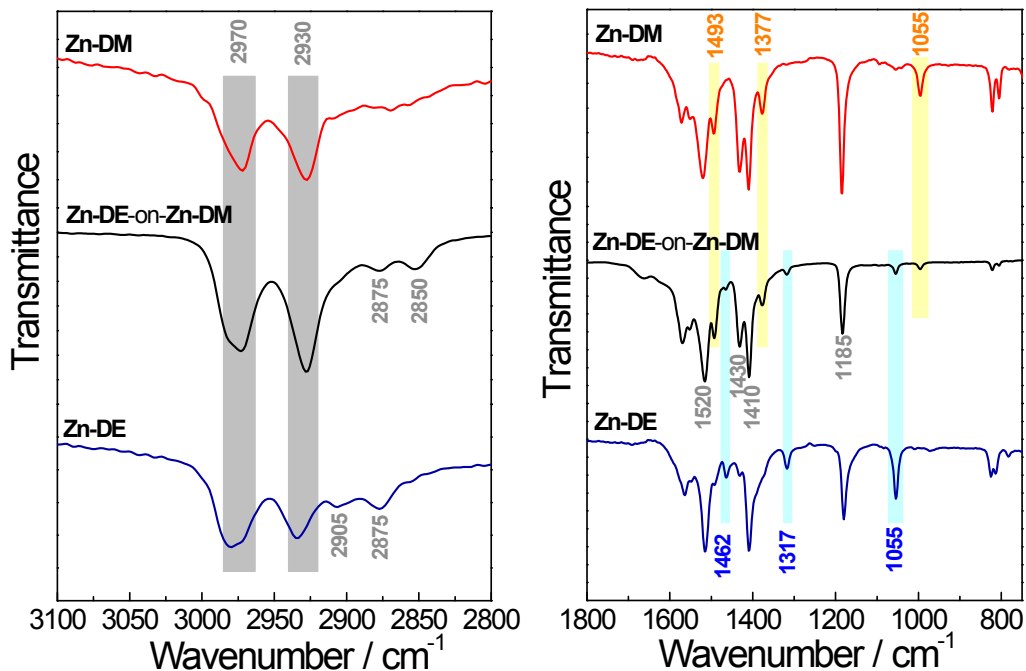


Figure S7 Example of IRRAS spectra of **Zn-DE-on-Zn-DM** heterostructured films indicates the position of the IR vibrational signals and the variation of relative transmittance at some wave numbers as a combination between the IRRAS spectra of the corresponding **Zn-DM** and **Zn-DE** MOF films.

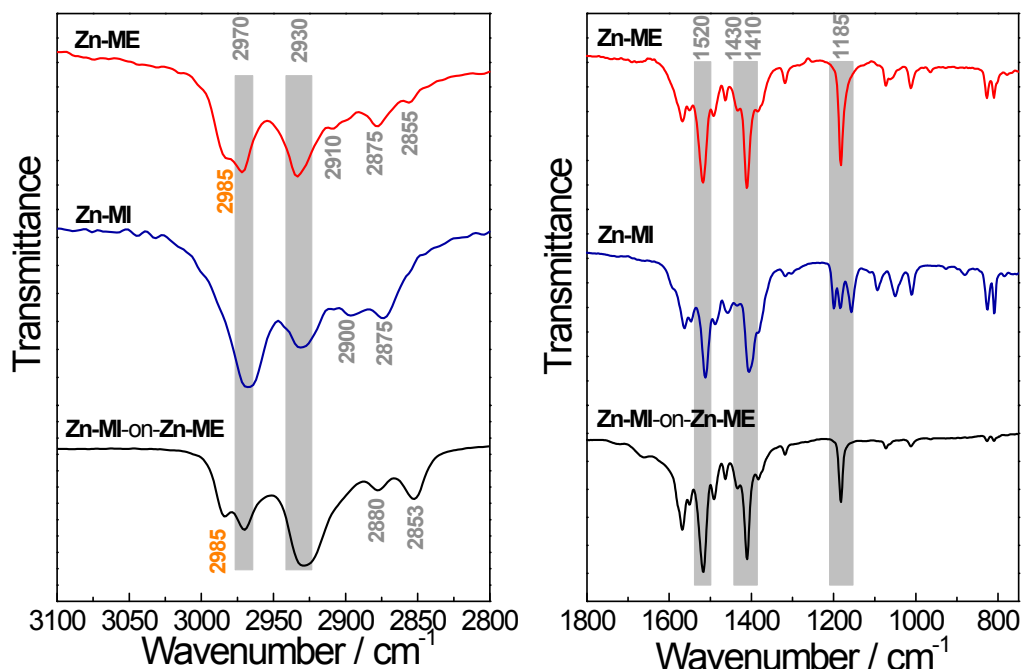


Figure S8 Example of IRRAS spectra of **Zn-MI-on-Zn-ME** heterostructured films indicates the position of the IR vibrational signals and the variation of relative transmittance at some wave numbers as a combination between the IRRAS spectra of the corresponding **Zn-ME** and **Zn-MI** MOF films.

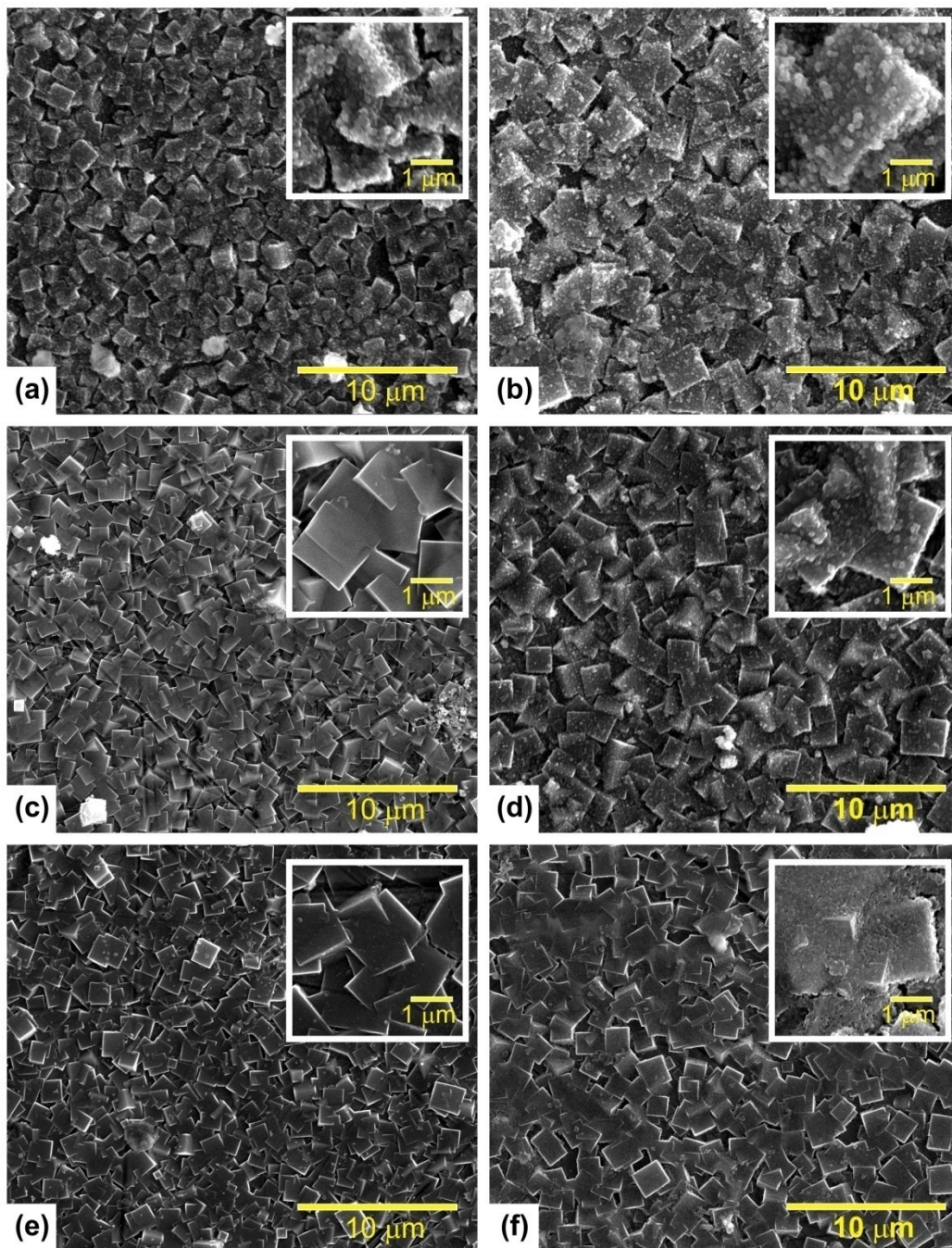


Figure S9 Scanning electron microscopy (SEM) images of the surfaces of the **Zn-MI-on-Zn-ME** and **Zn-DE-on-Zn-DM** heterostructured MOF thin films with different number of deposition cycles in each MOF component: (a) **Zn-MI(20)-on-Zn-ME(20)**, (b) **Zn-MI(20)-on-Zn-ME(30)**, (c) **Zn-DE(10)-on-Zn-DM(20)**, (d) **Zn-DE(20)-on-Zn-DM(20)**, (e) **Zn-DE(10)-on-Zn-DM(30)** and (f) **Zn-DE(20)-on-Zn-DM(30)**.

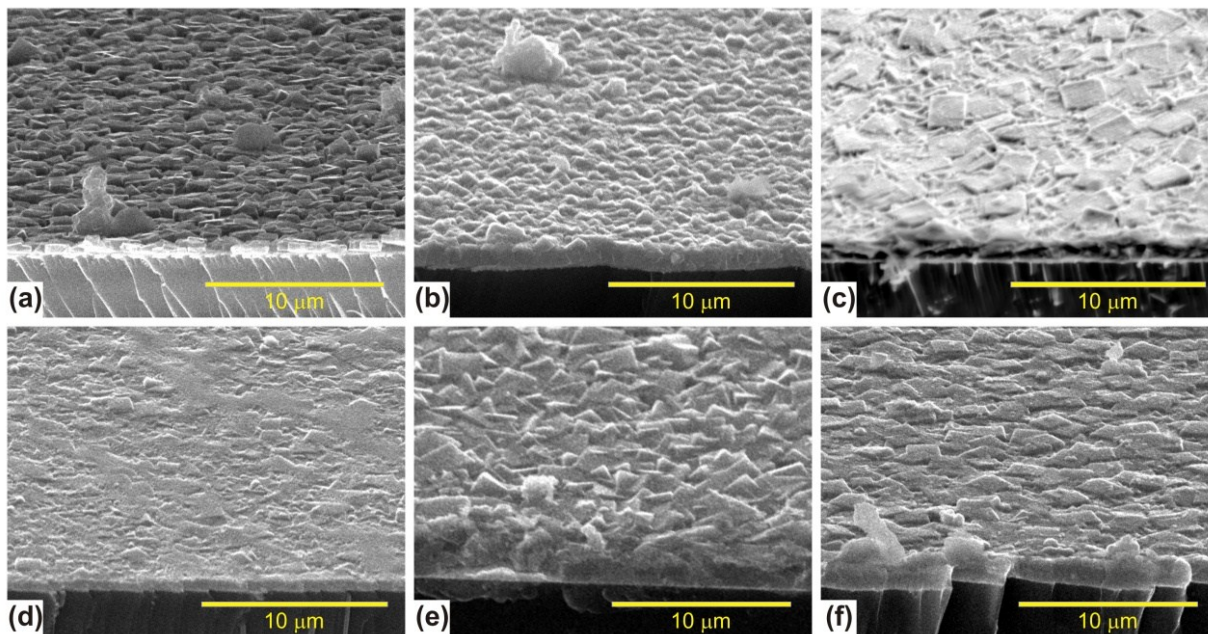


Figure S10 Cross section SEM images of the **Zn-MI-on-Zn-DM** heterostructured MOF thin films with different number of deposition cycles in each MOF component: (a) **Zn-MI(10)-on-Zn-DM(20)**, (b) **Zn-MI(15)-on-Zn-DM(20)**, (c) **Zn-MI(20)-on-Zn-DM(20)**, (d) **Zn-MI(10)-on-Zn-DM(30)**, (e) **Zn-MI(15)-on-Zn-DM(30)** and (f) **Zn-MI(20)-on-Zn-DM(30)**.

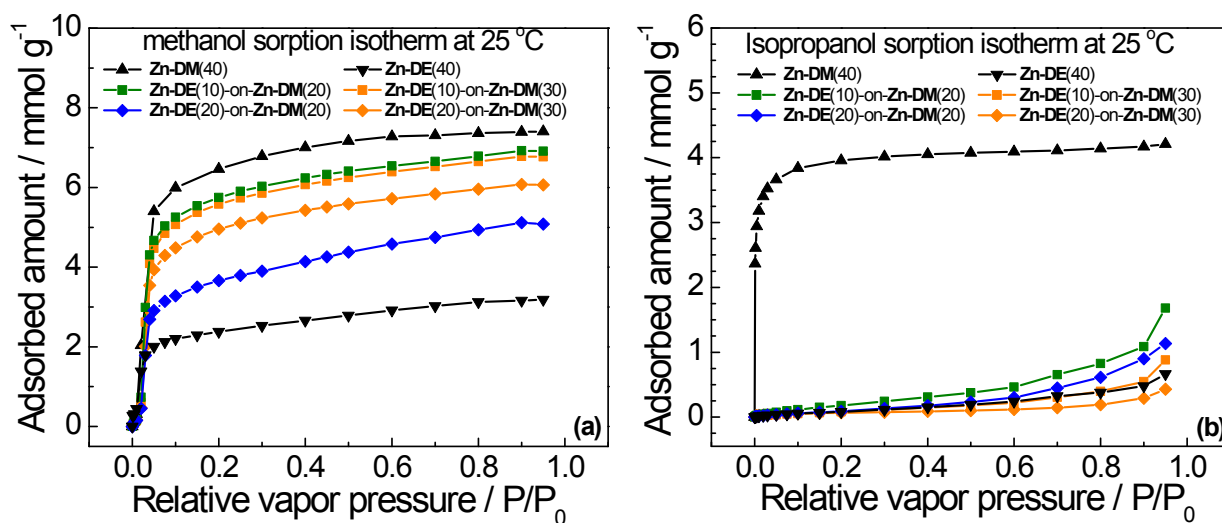


Figure S11 Single-component (a) methanol and (b) isopropanol adsorption isotherm at 25 °C using the environmentally controlled QCM of the **Zn-DE-on-Zn-DM** heterostructured films with various deposition cycles in each component in comparison with the corresponding **Zn-DM** and **Zn-DE** homostructured films.

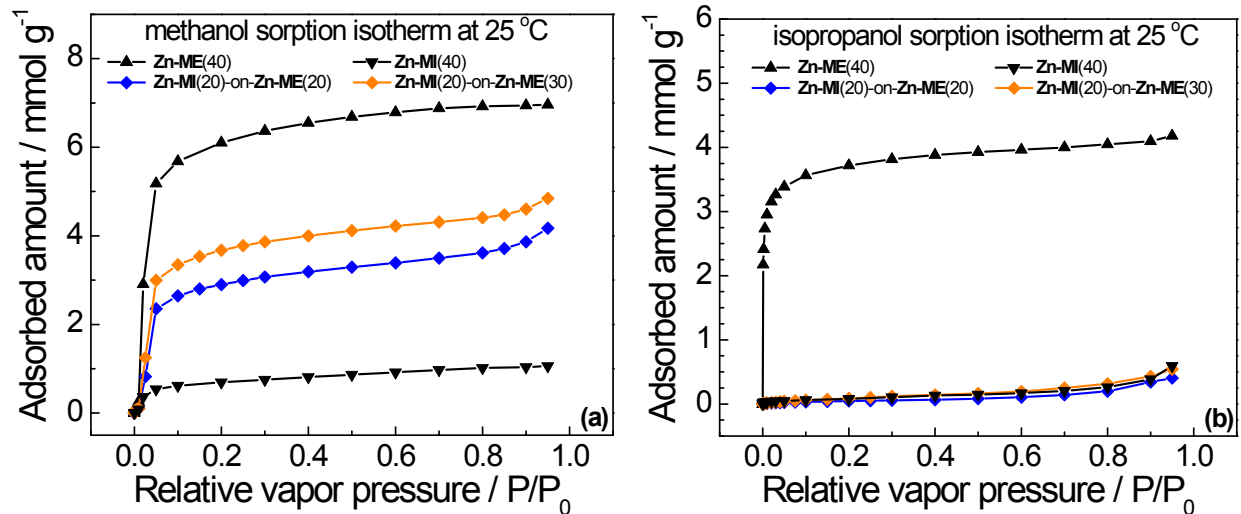


Figure S12 Single-component (a) methanol and (b) isopropanol adsorption isotherm at 25°C using the environmentally controlled QCM of the **Zn-MI-on-Zn-ME** heterostructured films with various deposition cycles in each component in comparison with the corresponding **Zn-ME** and **Zn-MI** homostructured films.

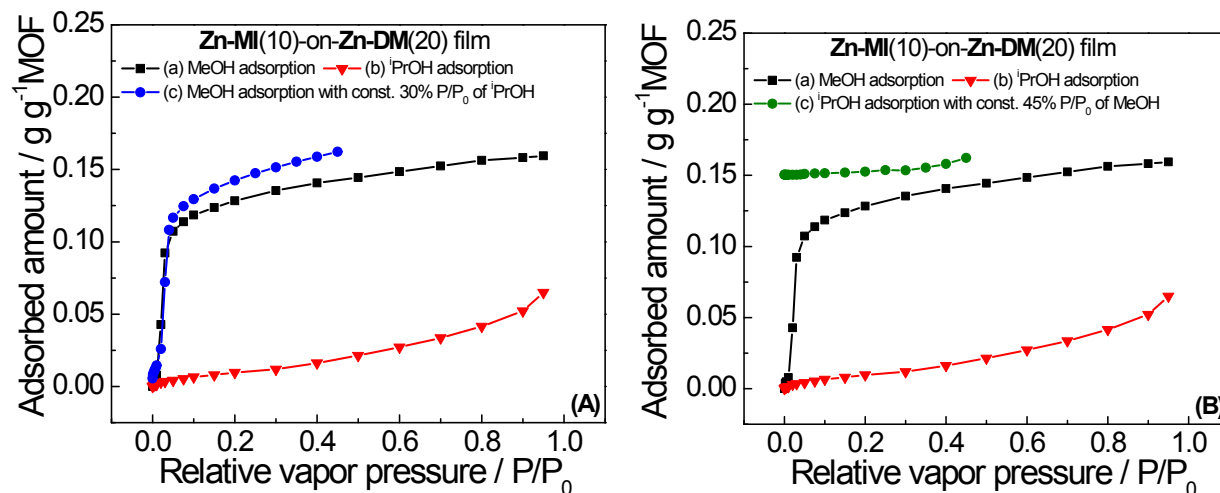


Figure S13 Methanol/isopropanol multi-components adsorption of the **Zn-MI(10)-on-Zn-DM(20)** heterostructured film at 25°C; (A) Methanol adsorption (P/P_0 varied from 0 to 45%) in the presence of constant 30% P/P_0 of isopropanol (blue) and (B) Isopropanol adsorption (P/P_0 varied from 0 to 45%) in the presence of constant 45% P/P_0 of methanol (green) in comparison with the single-component methanol (black) and isopropanol (red) adsorption isotherm at 25°C of the same sample.

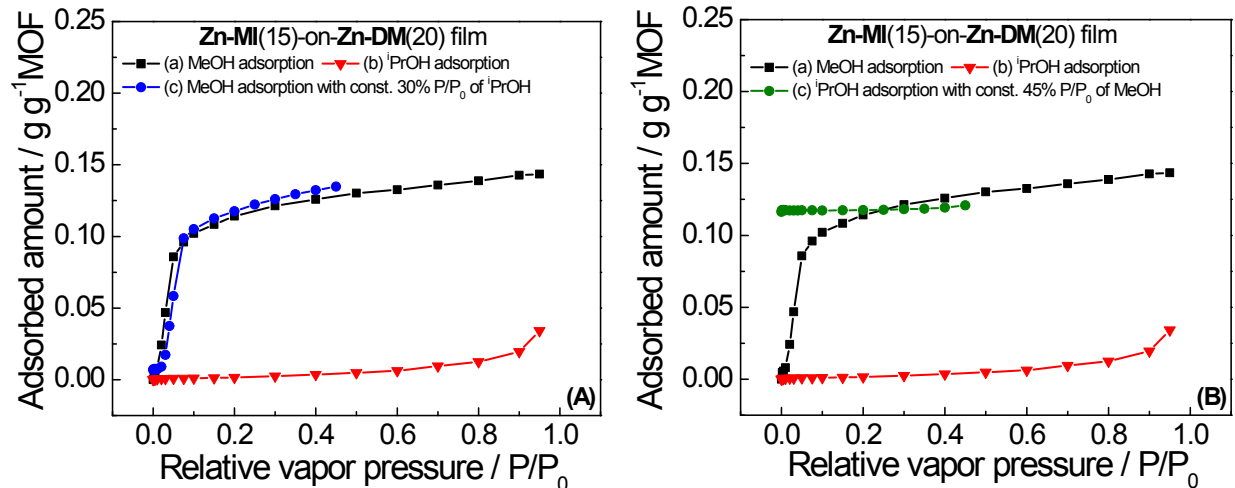


Figure S14 Methanol/isopropanol multi-components adsorption of the **Zn-MI(15)-on-Zn-DM(20)** heterostructured film at 25°C; (A) Methanol adsorption (P/P_0 varied from 0 to 45%) in the presence of constant 30% P/P_0 of isopropanol (blue) and (B) Isopropanol adsorption (P/P_0 varied from 0 to 45%) in the presence of constant 45% P/P_0 of methanol (green) in comparison with the single-component methanol (black) and isopropanol (red) adsorption isotherm at 25°C of the same sample.

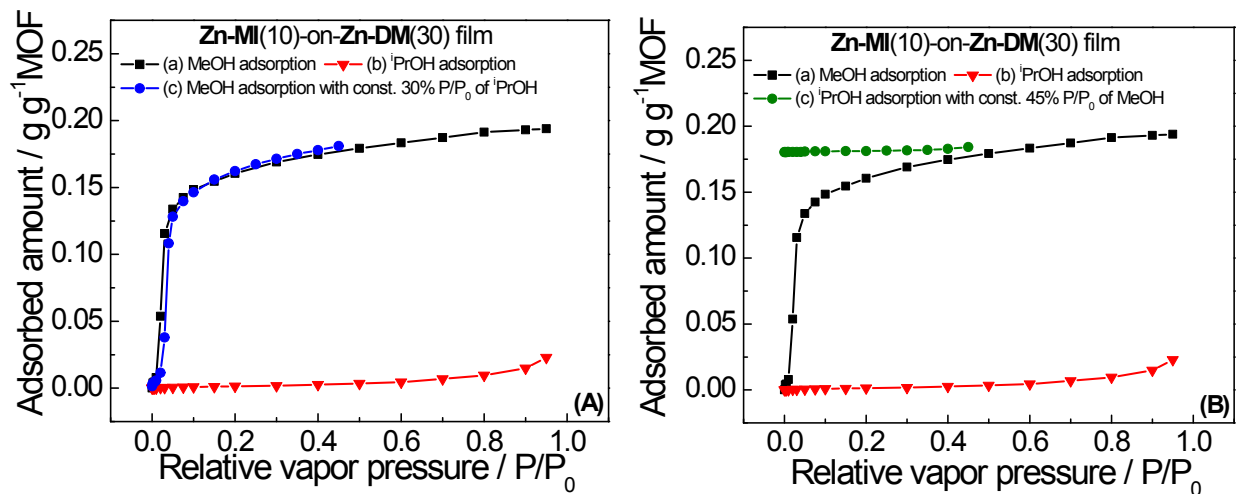


Figure S15 Methanol/isopropanol multi-components adsorption of the **Zn-MI(10)-on-Zn-DM(30)** heterostructured film at 25°C; (A) Methanol adsorption (P/P_0 varied from 0 to 45%) in the presence of constant 30% P/P_0 of isopropanol (blue) and (B) Isopropanol adsorption (P/P_0 varied from 0 to 45%) in the presence of constant 45% P/P_0 of methanol (green) in comparison with the single-component methanol (black) and isopropanol (red) adsorption isotherm at 25°C of the same sample.

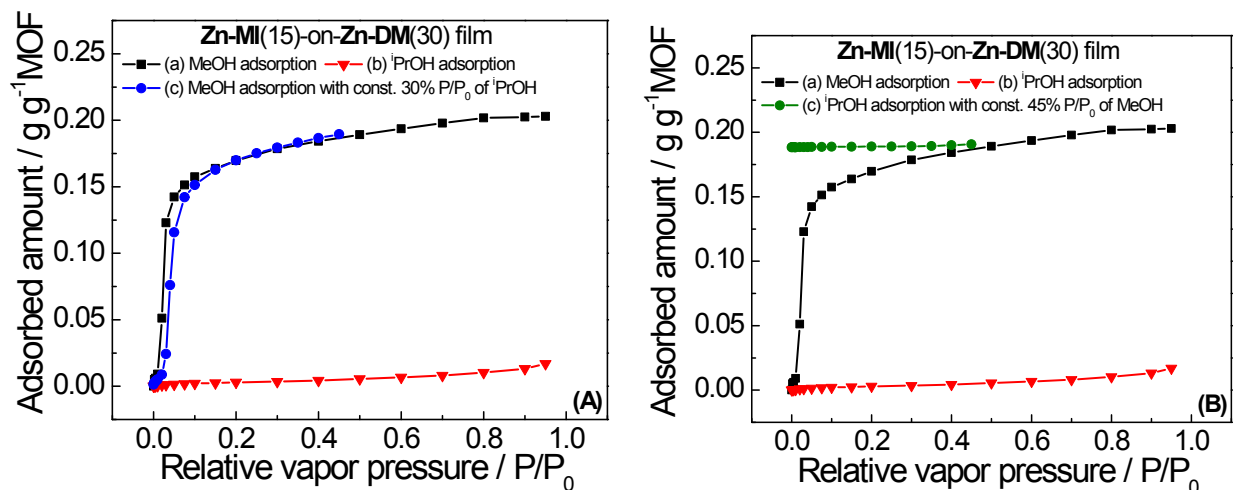


Figure S16 Methanol/isopropanol multi-components adsorption of the **Zn-MI(15)-on-Zn-DM(30)** heterostructured film at 25°C; (A) Methanol adsorption (P/P_0 varied from 0 to 45%) in the presence of constant 30% P/P_0 of isopropanol (blue) and (B) Isopropanol adsorption (P/P_0 varied from 0 to 45%) in the presence of constant 45% P/P_0 of methanol (green) in comparison with the single-component methanol (black) and isopropanol (red) adsorption isotherm at 25°C of the same sample.

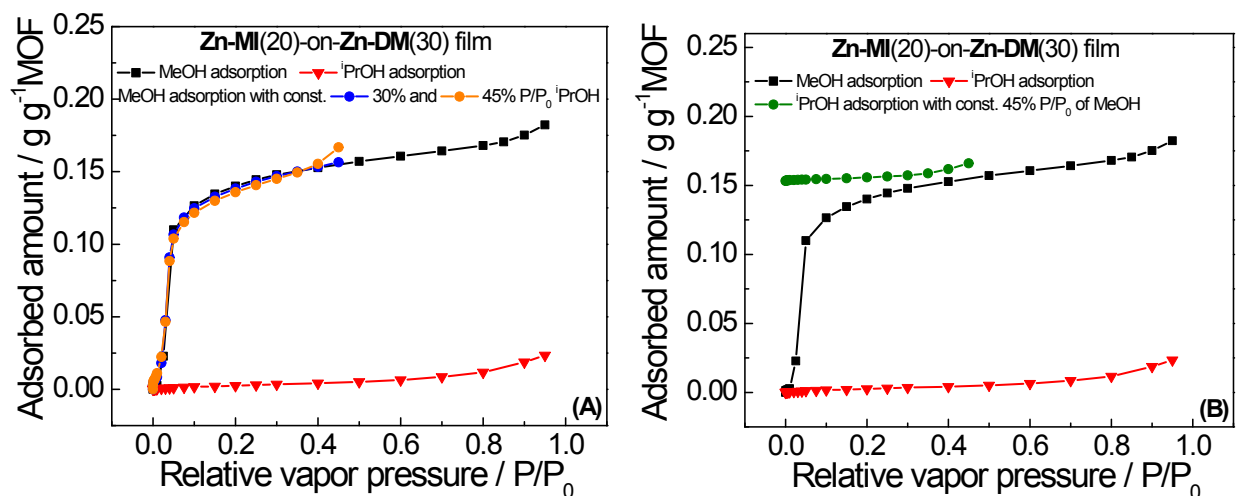


Figure S17 Methanol/isopropanol multi-components adsorption of the **Zn-MI(20)-on-Zn-DM(30)** heterostructured film at 25°C; (A) Methanol adsorption (P/P_0 varied from 0 to 45%) in the presence of constant 30% P/P_0 (blue) and 45% P/P_0 (orange) of isopropanol and (B) Isopropanol adsorption (P/P_0 varied from 0 to 45%) in the presence of constant 45% P/P_0 of methanol (green) in comparison with the single-component methanol (black) and isopropanol (red) adsorption isotherm at 25°C of the same sample.

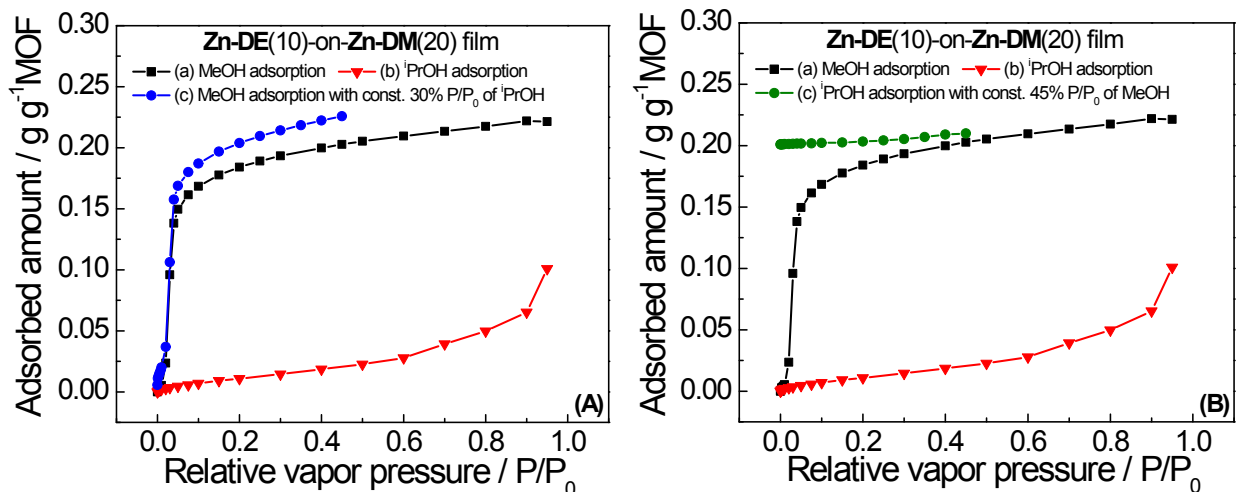


Figure S18 Methanol/isopropanol multi-components adsorption of the **Zn-DE(10)-on-Zn-DM(20)** heterostructured film at 25°C; (A) Methanol adsorption (P/P_0 varied from 0 to 45%) in the presence of constant 30% P/P_0 of isopropanol (blue) and (B) Isopropanol adsorption (P/P_0 varied from 0 to 45%) in the presence of constant 45% P/P_0 of methanol (green) in comparison with the single-component methanol (black) and isopropanol (red) adsorption isotherm at 25°C of the same sample.

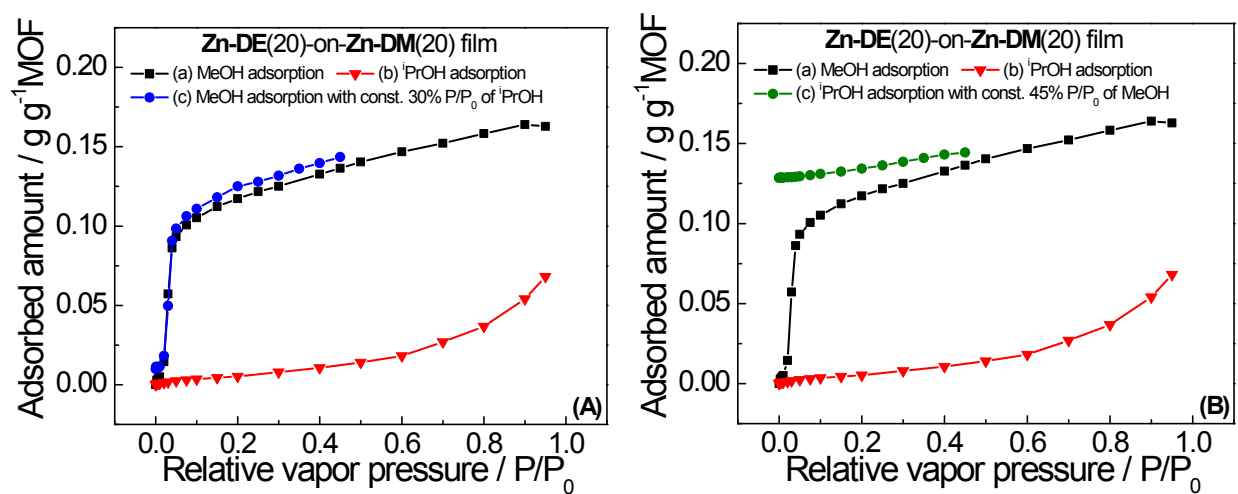


Figure S19 Methanol/isopropanol multi-components adsorption of the **Zn-DE(20)-on-Zn-DM(20)** heterostructured film at 25°C; (A) Methanol adsorption (P/P_0 varied from 0 to 45%) in the presence of constant 30% P/P_0 of isopropanol (blue) and (B) Isopropanol adsorption (P/P_0 varied from 0 to 45%) in the presence of constant 45% P/P_0 of methanol (green) in comparison with the single-component methanol (black) and isopropanol (red) adsorption isotherm at 25°C of the same sample.

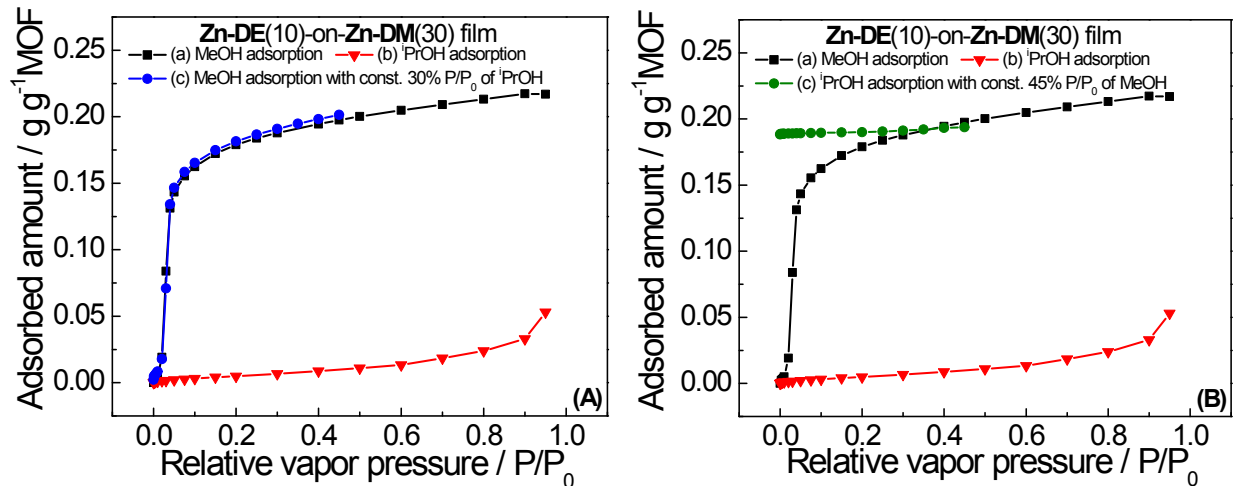


Figure S20 Methanol/isopropanol multi-components adsorption of the **Zn-DE(10)-on-Zn-DM(30)** heterostructured film at 25°C; (A) Methanol adsorption (P/P_0 varied from 0 to 45%) in the presence of constant 30% P/P_0 of isopropanol (blue) and (B) Isopropanol adsorption (P/P_0 varied from 0 to 45%) in the presence of constant 45% P/P_0 of methanol (green) in comparison with the single-component methanol (black) and isopropanol (red) adsorption isotherm at 25°C of the same sample.

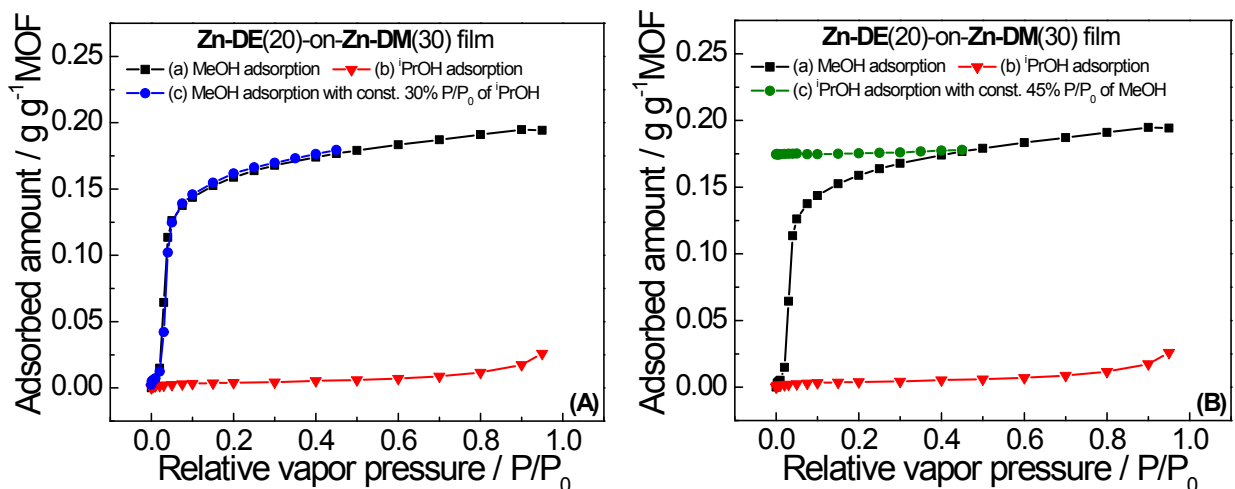


Figure S21 Methanol/isopropanol multi-components adsorption of the **Zn-DE(20)-on-Zn-DM(30)** heterostructured film at 25°C; (A) Methanol adsorption (P/P_0 varied from 0 to 45%) in the presence of constant 30% P/P_0 of isopropanol (blue) and (B) Isopropanol adsorption (P/P_0 varied from 0 to 45%) in the presence of constant 45% P/P_0 of methanol (green) in comparison with the single-component methanol (black) and isopropanol (red) adsorption isotherm at 25°C of the same sample.

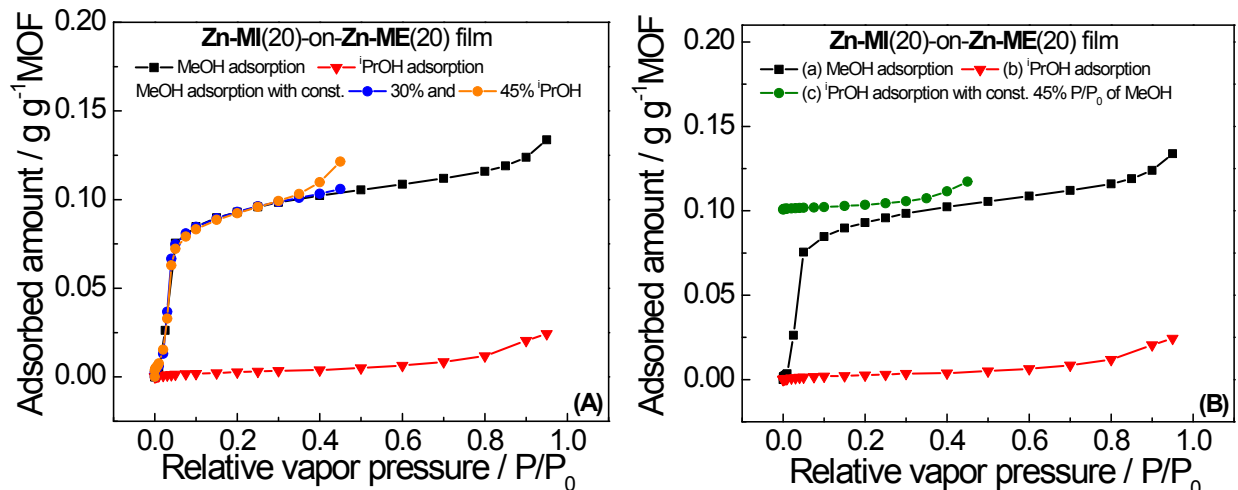


Figure S22 Methanol/isopropanol multi-components adsorption of the **Zn-MI(20)-on-Zn-ME(20)** heterostructured film at 25°C; (A) Methanol adsorption (P/P_0 varied from 0 to 45%) in the presence of constant 30% P/P_0 (blue) and 45% P/P_0 (orange) of isopropanol and (B) Isopropanol adsorption (P/P_0 varied from 0 to 45%) in the presence of constant 45% P/P_0 of methanol (green) in comparison with the single-component methanol (black) and isopropanol (red) adsorption isotherm at 25°C of the same sample.

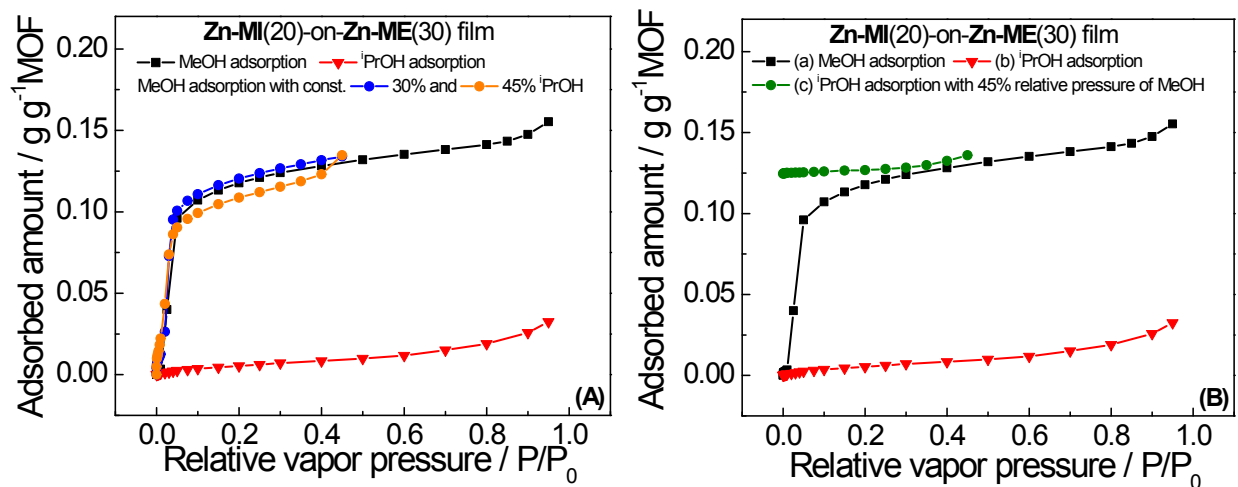


Figure S23 Methanol/isopropanol multi-components adsorption of the **Zn-MI(20)-on-Zn-ME(30)** heterostructured film at 25°C; (A) Methanol adsorption (P/P_0 varied from 0 to 45%) in the presence of constant 30% P/P_0 (blue) and 45% P/P_0 (orange) of isopropanol and (B) Isopropanol adsorption (P/P_0 varied from 0 to 45%) in the presence of constant 45% P/P_0 of methanol (green) in comparison with the single-component methanol (black) and isopropanol (red) adsorption isotherm at 25°C of the same sample.

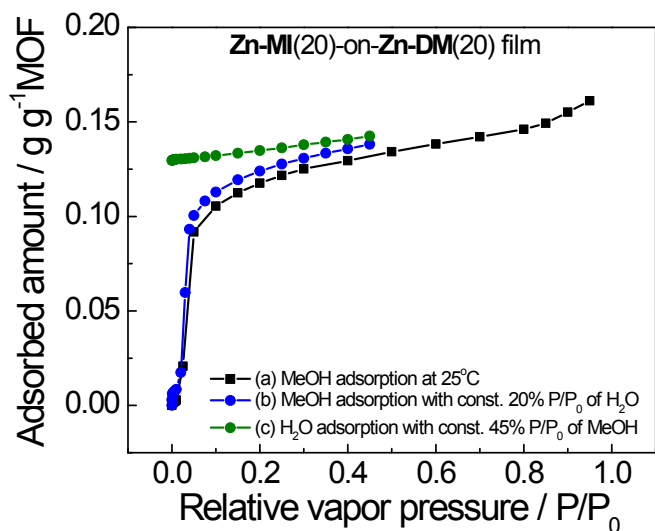


Figure S24 Methanol/moisture multi-components adsorption of the **Zn-MI(20)-on-Zn-DM(20)** heterostructured film at 25°C. Using the same sample, (a) single-component methanol (black) adsorption isotherm at 25°C, (b) methanol adsorption (P/P_0 varied from 0 to 45%) in the presence of constant 20% P/P_0 of moisture (blue) and (c) moisture adsorption (P/P_0 varied from 0 to 45%) in the presence of constant 45% P/P_0 of methanol (green) are compared.

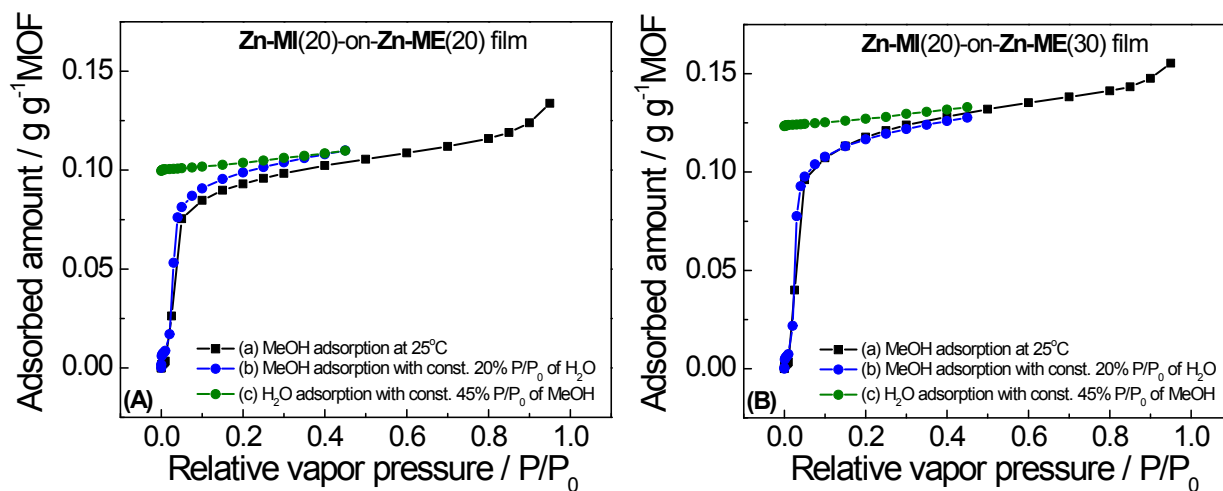


Figure S25 Methanol/moisture multi-components adsorption of the (A) **Zn-MI(20)-on-Zn-ME(20)** and (B) **Zn-MI(20)-on-Zn-ME(30)** heterostructured film at 25°C. Using the same sample, (a) single-component methanol (black) adsorption isotherm at 25°C, (b) methanol adsorption (P/P_0 varied from 0 to 45%) in the presence of constant 20% P/P_0 of moisture (blue) and (c) moisture adsorption (P/P_0 varied from 0 to 45%) in the presence of constant 45% P/P_0 of methanol (green) are compared.

References

- [1] G. Sauerbrey, *Z. Phys.*, 1959, **155**, 206-222.
- [2] C. Montoro, F. Linares, E. Q. Procopio, I. Senkowska, S. Kaskel, S. Galli, N. Masciocchi, E. Barea and J. A. R. Navarro, *J. Am. Chem. Soc.*, 2011, **133**, 11888–11891.